Tidal influence on seawater intrusion in unconfined coastal aquifers

Woei Keong Kuan,[1,2] Guangqiu Jin,[3] Pei Xin,[1] Clare Robinson,[4] Badin Gibbes,[5] and Ling Li[1,3]

Received 16 March 2011; revised 21 November 2011; accepted 6 December 2011; published 2 February 2012.

[1] Studies of seawater intrusion in unconfined coastal aquifers typically neglect oceanic oscillations such as tides and assume a static seaward boundary condition defined by the mean sea level. Laboratory experiments and numerical simulations were conducted to investigate the influence of tidal oscillations on the behavior of the saltwater wedge. For the conditions examined, the experiments showed that an upper saline plume formed in the intertidal zone due to tide-induced seawater circulation. The presence of the upper saline plume shifted the fresh groundwater discharge zone seaward to the low-tide mark and restricted the intrusion of the saltwater wedge. The overall seawater intrusion extent, as indicated by the wedge toe location, was reduced significantly compared with the nontidal (static) case. Results from the numerical model matched these experimental observations and further demonstrated the similar type of tidal influence on the saltwater wedge in a field-scale aquifer system. The Glover (1959) solution for predicting the saltwater wedge was modified to account for the tidal effect by including the tide-induced circulation as a "recharge" to the aquifer. The findings highlight the significant impact of the tide in modulating the groundwater behavior and salt-freshwater dynamics, not only within but also landward of the intertidal zone.

Citation: Kuan, W. K., G. Jin, P. Xin, C. Robinson, B. Gibbes, and L. Li (2012), Tidal influence on seawater intrusion in unconfined coastal aquifers, *Water Resour. Res.*, *48*, W02502, doi:10.1029/2011WR010678.

1. Introduction

[2] Coastal aquifers are often an important source of freshwater supply in coastal regions. Excessive groundwater extraction has led to seawater intrusion and water quality degradation in many coastal aquifers [*Bear et al.*, 1999; *Barlow and Reichard*, 2010]. The salinization of coastal aquifers will worsen with the increasing demands for freshwater resources in coastal areas and projected global sea level rise by 0.1 m to 2 m before 2100 [*Meier et al.*, 2007; *Pfeffer et al.*, 2008]. Better understanding of seawater intrusion in coastal aquifers and the ability to more accurately predict the extent of aquifer salinization is vital for improving water resources planning, development and management in coastal areas.

[3] Seawater intrusion in a coastal aquifer is a natural phenomenon that occurs due to flow and salt transport driven by the density difference between the seawater and fresh groundwater. The phenomenon is exacerbated by groundwater extraction and potentially sea level rise as these processes reduce the hydraulic gradient that drives fresh groundwater discharge to the ocean [*Werner and Simmons*, 2009; *Chang et al.*, 2011]. Various approaches, including analytical and numerical models, have been developed to explore and quantify seawater intrusion and the configuration of the saltwater wedge (SW) in coastal aquifers [e.g., *Reilly and Goodman*, 1985; *Bobba*, 1993; *Bear et al.*, 1999]. For example, the *Glover* [1959] solution is often used to delineate the SW in unconfined coastal aquifers with the discharging fresh groundwater overlying the intruded higher density seawater. This solution is based on the assumption of a sharp salt-freshwater interface (SFI) and is given by:

$$x_{w,F} = \frac{Q_F}{2\gamma K} \tag{1}$$

$$x_{I,F} = -(z^2 - 4x_{w,F}^2)\frac{\gamma K}{2Q_F}, \tag{2}$$

where $x_{w,F}$ [L] is the horizontal width of the freshwater outflow zone on the seabed; Q_F [$L^2\ T^{-1}$] is the fresh groundwater discharge rate per unit width of the aquifer; γ [−] is the excess of the specific gravity of seawater over freshwater given by $(\rho_s - \rho_f)/\rho_f$, with ρ_s [ML^{-3}] and ρ_f [ML^{-3}] representing the density of saltwater and freshwater, respectively; K [LT^{-1}] is the hydraulic conductivity of the aquifer; and $x_{I,F}$ [L] is the landward distance of the SFI from the mean shoreline at an aquifer depth of z [L]. The Glover solution describes how seawater intrusion is controlled by the balance between the regional hydraulic gradient, associated with the fresh groundwater discharge,

[1]National Centre for Groundwater Research and Training, School of Civil Engineering, University of Queensland, St. Lucia, Queensland, Australia.
[2]Faculty of Civil Engineering, Universiti Teknologi MARA, Selangor, Malaysia.
[3]State Key Laboratory of Hydrology, Water Resources and Hydraulic Engineering, Hohai University, Nanjing, China.
[4]Department of Civil and Environmental Engineering, University of Western Ontario, London, Ontario, Canada.
[5]School of Civil Engineering, University of Queensland, St. Lucia, Queensland, Australia.

0043-1397/12/2011WR010678

and hydraulic head difference caused by the density variation. Diffusive models that consider coupled density-dependent flow and salt transport have also been developed to examine seawater intrusion governed by essentially the same balance principle [*Bear and Alexander*, 2010]. Most previous studies focused on the effects of, for example, groundwater extraction and recharge on the saltwater wedge and assumed a static seaward boundary defined by the mean sea level. Accurate prediction however relies on proper understanding of the interactions between the aquifer and coastal sea. While oceanic oscillations including tides are ubiquitous on coastlines worldwide and are known to influence the groundwater behavior, the effect of these oscillations on seawater intrusion is not well understood.

[4] Tidal oscillations propagate in coastal aquifers, causing groundwater head fluctuations. These fluctuations have been studied extensively with observations and groundwater wave theories established [*Lanyon et al.*, 1982; *Nielsen*, 1990; *Li et al.*, 1997; *Turner et al.*, 1997; *Robinson et al.*, 1998]. Generally the fluctuations are significant near the shore but are attenuated with increasing time lag as they propagate inland. Recent studies have shown that tidal oscillations acting on a sloping beach induce relatively rapid seawater circulation in the intertidal zone below the beach surface [*Robinson et al.*, 2006; *Xin et al.*, 2010]. Salt transport associated with this seawater circulation leads to the formation of an upper saline plume (USP) within the intertidal zone. The presence of the USP alters the salt distribution in the near-shore aquifer with fresh groundwater discharging in a zone between the USP and the (lower) SW [*Boufadel*, 2000; *Robinson et al.*, 2006; *Dale and Miller*, 2007; *Vandenbohede and Lebbe*, 2007; *Robinson et al.*, 2007c]. While the significant influence of tides on the flow and salt distribution in the intertidal zone has been reported [*Robinson et al.*, 2007a], the tidal effect on the extent of aquifer salinization landward of the intertidal zone is unclear.

[5] Few studies have examined the effects of tides on saltwater intrusion with conflicting findings. *Inouchi et al.* [1990] investigated the influence of tides on a confined coastal aquifer using both an analytical and a numerical model. They found that tides only influenced the SW near the shore. *Ataie-Ashtiani et al.* [1999] and *Chen and Hsu* [2004] examined the influence of tidal oscillations on seawater intrusion in shallow unconfined aquifers. Both studies suggested that tides forced seawater to intrude further inland and created a more dispersed SFI across the intertidal zone. These results were based on numerical simulations of a shallow aquifer (aquifer thickness, $H = 7$ m) subject to tidal fluctuations with amplitudes of 1 m [*Ataie-Ashtiani et al.*, 1999] and 3 m [*Chen and Hsu*, 2004]. More recently, *Werner and Lockington* [2006] and *Mao et al.* [2006] investigated numerically the effects of tidal fluctuations on near-shore groundwater flow and salt transport. *Werner and Lockington* [2006] showed that tides acting on a vertical seaward boundary led to a more dispersed SFI but reported no significant changes in the landward extent of the SW. On the other hand, *Mao et al.* [2006] indicated that tides acting on a mildly sloping beach increased the total distance of seawater intrusion into the aquifer. The numerical models for both studies used a fixed head condition at the landward boundary. In contrast, the numerical study of intertidal flow dynamics by *Robinson et al.* [2007a] used a fixed flux condition at the landward boundary and reported that tides led to a significant reduction of the overall extent of seawater intrusion in a simulated unconfined aquifer.

[6] This study aimed to clarify the tidal effects on the behavior of the SW in unconfined aquifers through both laboratory and numerical experiments. The tidal influence was examined relative to the forcing of the inland fresh groundwater discharge and density-induced seawater circulation. Laboratory experiments were conducted in a sand flume under well controlled conditions using dye to trace the salt distribution under conditions of no tides and tides of varying tidal amplitudes and with different inland freshwater fluxes. The collected data was used to test a numerical model developed in SUTRA [*Voss and Provost*, 2002] through calibration and sensitivity analyses. This model was then used to simulate the tidal influence on the SW in a larger-scale (field-scale) aquifer system to further illustrate the phenomena observed in the laboratory experiments. The experimental and numerical results were applied to develop a modified Glover solution to characterize the combined effects of fresh groundwater discharge, density-driven flow and tide-induced circulation on saltwater intrusion in unconfined coastal aquifers.

2. Methodology

2.1. Laboratory Experiments

2.1.1. Experimental Setup and Measurements

[7] Experiments were conducted in a 3.5 m (long) $\times$ 0.8 m (high) $\times$ 0.02 m (wide) sand flume, constructed from 12 mm thick tempered glass mounting on an adjustable steel platform (Figure 1a). The sand flume was divided into three compartments: two reservoirs at both ends containing freshwater and saltwater, representing the landward and seaward boundary, respectively; and a middle compartment packed with quartz sand to simulate an unconfined coastal aquifer bounded by a sloping beach surface (slope $= 0.263$). The grain size distribution of the sand was relatively uniform with $d_{50} = 0.24$ mm and $d_{90}/d_{10} = 2.86$. The saturated hydraulic conductivity of the porous medium was measured between 5.2×10^{-3} and 5.9×10^{-3} m s^{-1} with a mean of 5.5×10^{-3} m s^{-1} and a standard deviation of 0.3×10^{-3} m s^{-1}, using an in-situ method based on steady flows. The porosity of the sand was also measured with an average value of 0.46 using the imbibition method [*Collins*, 1961]. The experimental setup was essentially two-dimensional, focusing on flow and salt transport processes in the vertical and cross-shore direction.

[8] The landward reservoir was supplied with freshwater at a fixed rate simulating a fixed freshwater flux from the landward boundary to the aquifer. A fixed flux instead of a fixed head condition was applied to avoid the tidal influence on the freshwater discharge rate due to tide-induced water table overheight [*Nielsen*, 1990; *Ataie-Ashtiani et al.*, 1999]. At the seaward end, two saltwater tanks were used to supply saltwater to the reservoir and near-shore zone. Under the nontidal condition, saltwater was supplied from one tank (60 L, Figure 1a) at a preset rate (greater than the freshwater discharge rate) and discharged through an overflow outlet to maintain a constant salinity and water level (mean sea level, MSL) in the near-shore zone. Under

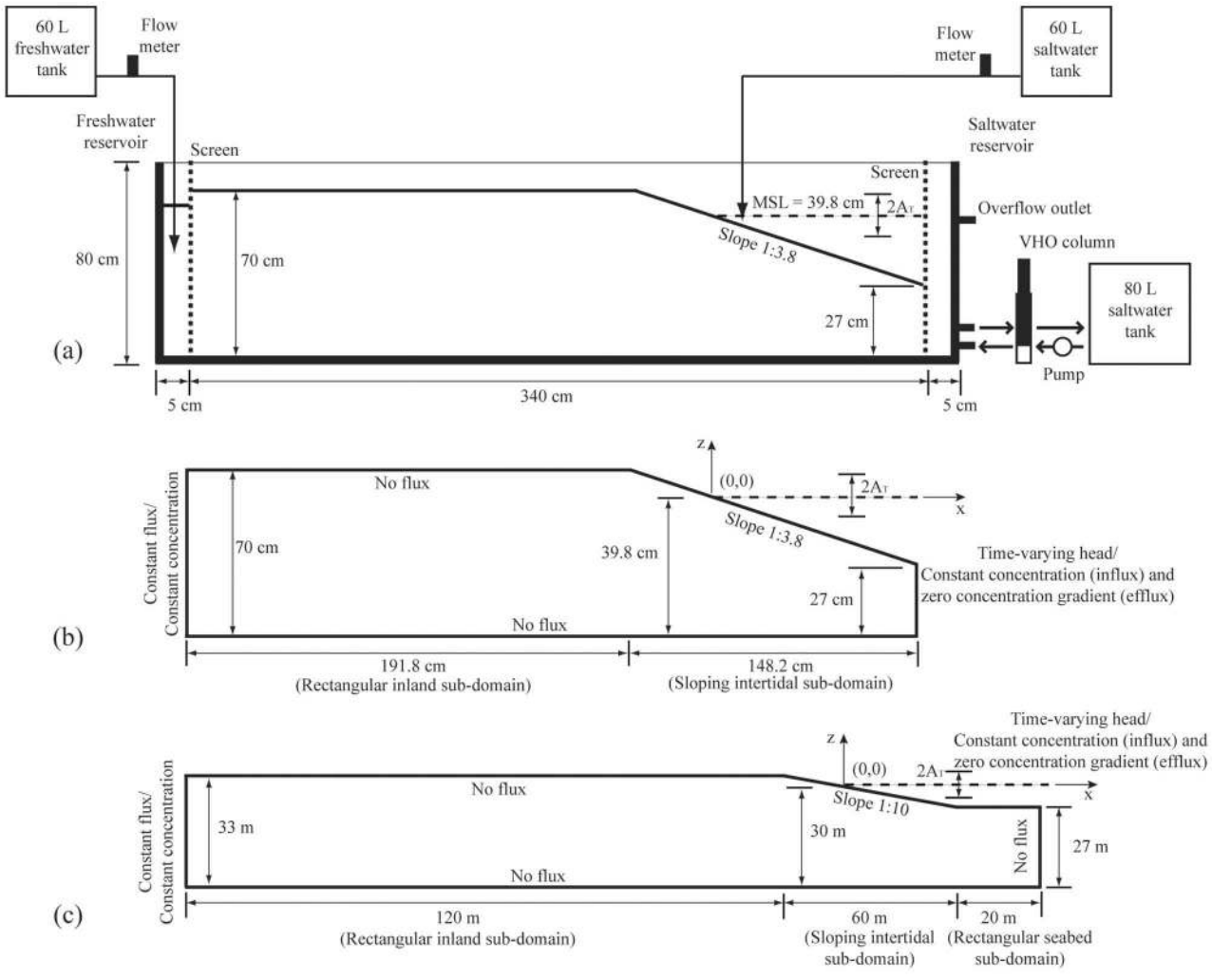

Figure 1. Schematic of the (a) experimental setup, and (b) laboratory-scale and (c) field-scale numerical model setup including the boundary conditions adopted.

the tidal condition, a second tank (80 L) was used to pump saltwater into and out of the near-shore zone via a variable height overflow (VHO) column to generate simple sinusoidal tides (further details of the tidal generation method can be found in the work of *Cartwright et al.* [2003, 2004]). During the experiments, both the salinity and water level in the near-shore zone were monitored.

[9] The saltwater solution was prepared by dissolving 33.4 g of sodium chloride (NaCl, AR grade) and 1.6 g of FD&C red food dye (ROHA Dyecem Pvt Ltd) in a liter of deionized water. Food dye has been used successfully as a tracer in previous studies of variable-density flows [*Zhang et al.*, 2002; *Goswami and Clement*, 2007; *Luyun et al.*, 2009]. Sorption tests following the method of *Goswami and Clement* [2007] were conducted to confirm the inert property of the dye in the interaction with the porous medium (i.e., no sorption of the dye by the sand). The density of the salt solution was measured at 1.026 g ml^{-1} using a specific gravity hydrometer (Carlton Glass Co. Pty. Ltd., BS718), and this was controlled throughout the experiments.

[10] High-resolution digital photographs were taken at interval of 15 s to track the saltwater intrusion in the sand flume throughout the experiments. The color photographs were converted to gray scale images, which were further processed in a binary fashion by setting pixels with luminance levels greater than 0.5 to white and the remaining pixels to black. These black-white images allowed consistent delineation of the interface between the freshwater (white) and saltwater (black) in the aquifer.

2.1.2. Experimental Procedure and Cases

[11] Prior to the experiment, the sand flume was filled with deionized water. A steady state flow was established with a constant discharge of 20 mL min^{-1} (or 15 mL min^{-1} in another experiment) deionized water into the freshwater reservoir. The water level at the seaward side was maintained at 45.0 cm (~5.0 cm higher than the MSL) above the tank bottom. For the tidal cases, saltwater was then introduced into the saltwater reservoir through the VHO column to simulate a coastal sea subject to single constituent tidal oscillations. The experiment was continued until the flow and salt distribution reached a quasi steady (periodic) state. For the nontidal case, saltwater was fed to the

saltwater reservoir with the VHO column disconnected to maintain a constant MSL.

[12] Six experiments were conducted to examine saltwater intrusion in the aquifer under conditions of three different tidal amplitudes (4.2, 3.2 and 5.2 cm) and two inland freshwater discharge rates (20 and 15 mL min^{-1}) (Table 1). A nontidal experiment was conducted for each inland freshwater discharge rate.

2.2. Numerical Simulations

[13] The variably saturated variable-density groundwater flow code, SUTRA [*Voss and Provost*, 2002] was used to simulate the experiments under the different tidal and inland flow conditions. In SUTRA, variably saturated, variable-density flow is governed by the Richards equation, with density terms coupled with the solute transport equation [*Voss and Provost*, 2002]. The constitutive relationships between the hydraulic conductivity, soil saturation and capillary pressure head are given by the *van Genutchen* [1980] functions. The model simulates a vertical cross-shore aquifer section, assuming negligible flow and solute transport in the alongshore direction (Figure 1b). This is consistent with the experimental setup.

[14] No areal recharge or evapotranspiration was considered and hence there was no water or solute flux across the top boundary (Figure 1b). The aquifer base was set to be impermeable (zero flux). The landward boundary was set as a fixed flux boundary with zero solute concentration. The seaward boundary condition varied with the tidal level that fluctuated according to

$$h(t) = z_{MSL} + A_T \sin(\omega t), \tag{3}$$

where h [L] is the tidal level at the time t [T]; z_{MSL} [L] is the mean sea level; A_T [L] is the tidal amplitude and ω [T^{-1}] is the tidal angular frequency. The seaward boundary section below the sea surface was subjected to the hydrostatic pressure given by the seawater depth and thus set as a specified-pressure boundary. The section above the sea surface was treated according to the following two conditions: (1) if the (exposed) nodes were saturated at the previous time step, they were taken as part of a seepage face with pressure equal to zero (atmospheric pressure); and (2) if the nodes were unsaturated at the previous time step, they were treated as a no-flow boundary [*Xin et al.*, 2010].

Table 1. Cases for Experiments and Numerical Simulations Performed for Laboratory- and Field-Scale Models

Laboratory-Scale	NT-Q1	NT-Q2	A1-Q1	A1-Q2	A2-Q1	A3-Q1
	Input conditions					
Q_F (ml min^{-1})	20	15	20	15	20	20
A_T (cm)	–	–	4.2	4.2	3.2	5.2
Tidal period (sec)	–	–	62	62	62	62
Freshwater conc. (ppt)	0	0	0	0	0	0
Saltwater conc. (ppt)	35.0	35.0	35.0	35.0	35.0	35.0

Field-Scale (FS-)	NT-Q1	NT-Q2	A1-Q1	A1-Q2
	Input conditions			
Q_F (m^3 d^{-1})	0.210	0.105	0.210	0.105
A_T (m)	–	–	1.0	1.0
Tidal period (h)	–	–	12	12
Freshwater conc. (ppt)	1.0	1.0	1.0	1.0
Saltwater conc. (ppt)	35.0	35.0	35.0	35.0

For salt transport, the seawater concentration was set to be constant at 35 ppt (mass fraction, parts per thousand) for inflow to the aquifer and zero concentration gradient was specified for outflow from the aquifer (Figure 1b).

[15] Typical values of the soil water retention parameters for sand were adopted [*Carsel and Parrish*, 1988]. In simulating the experiments, the model was further calibrated by adjusting values of hydraulic conductivity, dispersivity (longitudinal and transverse), parameter a in the *van Genutchen* [1980] function and porosity to match the observations.

[16] Tests were conducted to ensure that the numerical solutions were converged and independent of the time step and mesh size. All simulations were run until such time that the numerical solutions had reached the quasi-steady state with respect to both hydraulic head and salt concentration.

3. Results and Discussion

3.1. Experimental Results

[17] The color images taken from the sand flume experiments at the (quasi) steady state are shown in Figure 2. The range of vertical axis (z) for all study cases is identical with the same MSL located at 0.398 m above the bottom of tank (Figure 2). As indicated by the sharp change (fade) of color, a distinct separation of the freshwater and saltwater (red) was observed. The low mixing intensity was expected given the relatively uniform size distribution of sands used and the small flume width. This is also consistent with observations from previous experiments using a similar sand flume setup under the nontidal condition [*Goswami and Clement*, 2007; *Abarca and Clement*, 2009]. The SFI was defined based on a critical value of 0.5 for the luminance and relative salt concentration to facilitate further analyses of the experimental and numerical results, respectively (summarized in Table 3a).

[18] Under the nontidal condition and freshwater discharge rate of 20 mL min^{-1} (NT-Q1), saltwater intruded the initially fresh aquifer from the seaward boundary, forming a SW that progressively moved inland until it reached steady state after approximately 720 min. At the steady state, the toe of the wedge was located at a distance of ~52 cm landward from the mean shoreline (MS, Figure 2a). The upper edge (UE) of the wedge intercepted with the beach surface at ~8.5 cm seaward of the MS. Landward of this edge was the freshwater discharge zone (FDZ) with a width of ~8.9 cm across the sloping boundary.

[19] In the case with the tide (A1-Q1), saltwater intruded the initially fresh aquifer through both the seaward vertical boundary and the sloping beach surface in the intertidal zone. This resulted in two saline zones separated by the FDZ – an USP in the intertidal zone in addition to the lower SW (Figure 3). The tidal oscillations generated hydraulic gradients across the sloping beach surface, which led to a circulating flow system with seawater infiltrating the upper part of the beach and exfiltrating from the lower intertidal zone. This circulation resulted in the formation of the USP initially close to the beach surface and expanding downward to a quasi-steady, nearly half-elliptic shape that matched the circulation pattern. The evolution of this saline plume was relatively rapid, with the quasi-steady state reached in 60 min (~58 tidal cycles; Figure 3d). In contrast, the encroachment of the SW occurred more gradually

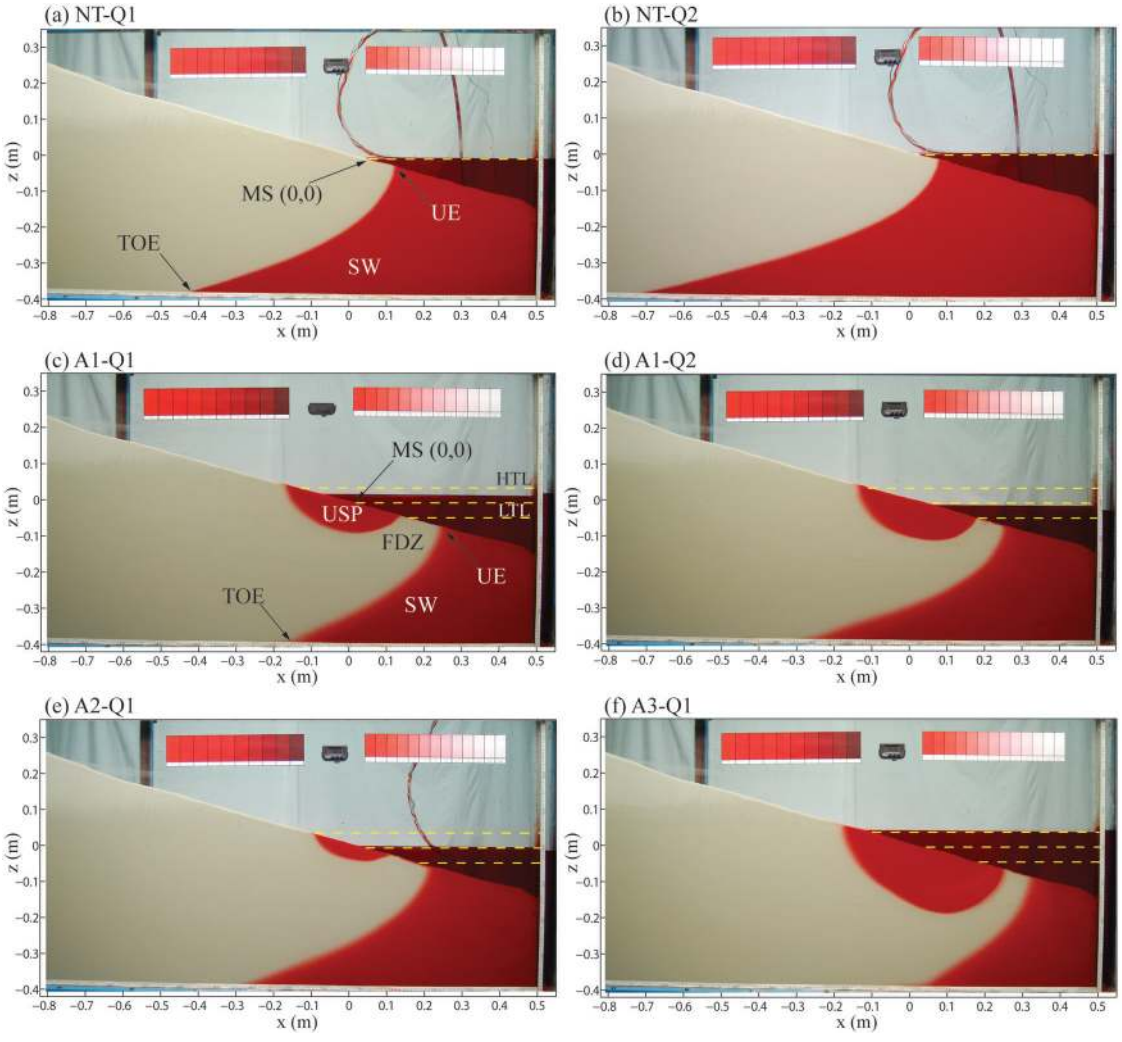

Figure 2. Images of the salt distribution in the sand flume for different experimental cases at the steady and quasi-steady state. The lower saltwater wedge (SW), toe of the saltwater wedge (TOE), upper edge of the saltwater wedge (UE), upper saline plume (USP), freshwater discharge zone (FDZ), mean shoreline (MS), high tide level (HTL) and low tide level (LTL) are denoted.

with the quasi-steady state condition achieved after ~330 min (Figure 3h); after that the experiment was continued for another 90 min (Figure 3i).

[20] The salt distribution in the tidally influenced aquifer at the quasi-steady state, characterized by two saline zones confining a FDZ, is consistent with previous numerical results and field observations [*Boufadel*, 2000; *Vandenbohede and Lebbe*, 2006; *Robinson et al.*, 2007a]. In presence of the USP, the SW toe stopped at ~18.9 cm landward from the MS, 33.1 cm shorter than that for the nontidal case (NT-Q1; Table 3a). The UE of the SW was pushed seaward to below the low tide mark, approximately 22.9 cm from the MS (Figure 2c; Table 3a). The FDZ on the beach surface was also shifted seaward and widen by 2.2 cm (i.e., 11.1 cm wide c.f. 8.9 cm for the nontidal case). These laboratory results indicated that the formation of the USP reduced the landward encroachment of the SW.

[21] The tidal effect on the SW was moderated by the magnitude of the freshwater discharge. In cases NT-Q2 (nontidal) and A1-Q2 (tidal), the wedge intruded further inland due to the reduced freshwater discharge (Figures 2b and 2d; Table 3a). Without the tide, the toe of the SW moved 27.3 cm further inland compared with case NT-Q1. For the tidal conditions, the formation for the USP again constrained the intrusion extent, with the wedge toe reaching only 33.4 cm from the MS. While this also represented an increased intrusion distance by 14.5 cm compared with the high freshwater discharge case (A1-Q1), the extent of the increase was smaller than the difference between the nontidal cases. The influence of the tide (with the same amplitude) on the saltwater intrusion appeared to be more significant for a smaller freshwater discharge rate. This is because the tidal circulations in the intertidal zone and thus the USP expanded laterally and vertically as the freshwater discharge decreased (Figure 2d; Table 3a). Such response of the USP to changes of the freshwater discharge rate has been observed in previous numerical simulations [*Robinson et al.*, 2007a].

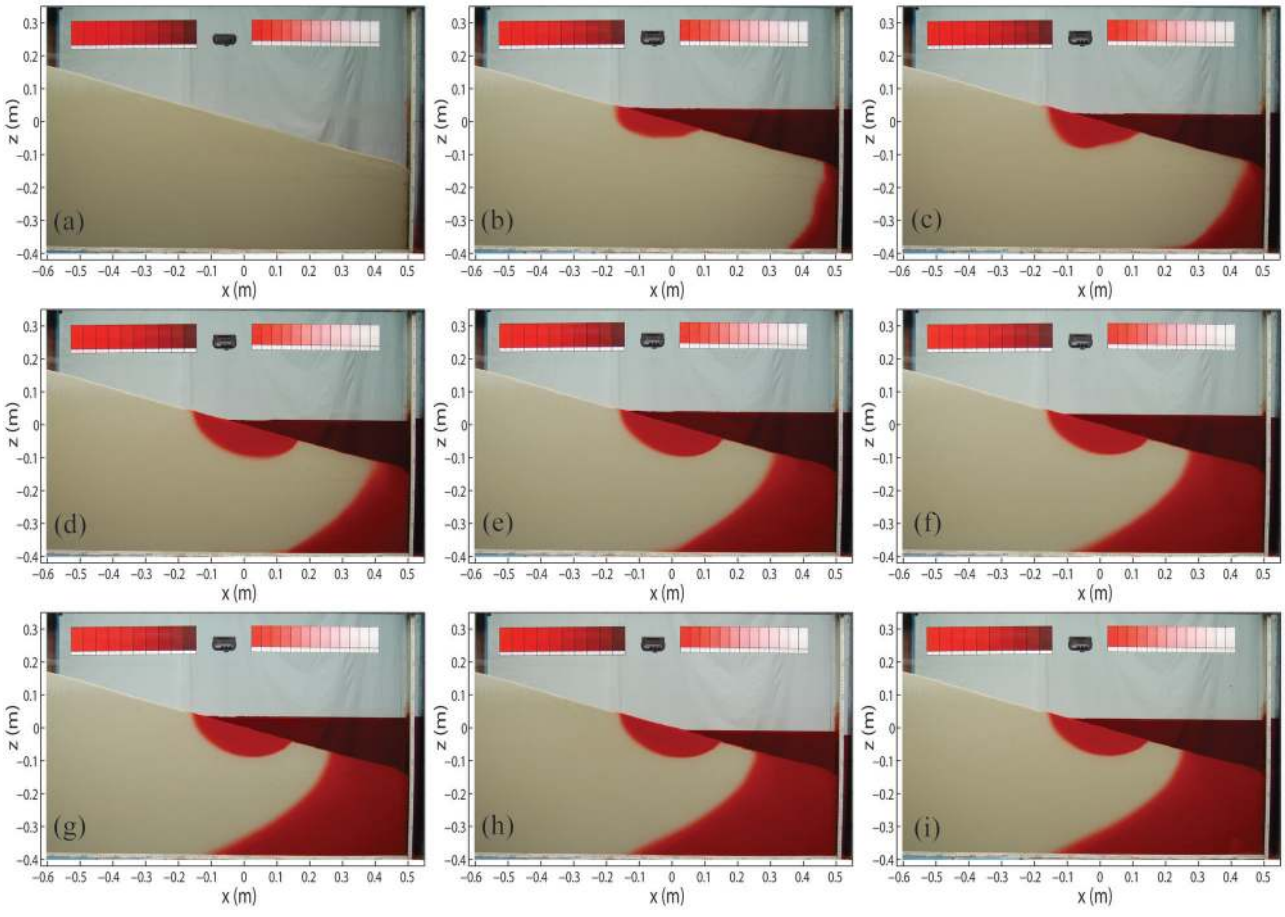

Figure 3. Transient development of the saltwater wedge and upper saline plume for case A1-Q1. The photos were taken at times (a) 0, (b) 15, (c) 30, (d) 60, (e) 120, (f) 180, (g) 240, (h) 330, (i) 420 min from the beginning of the experiment, respectively.

[22] Variations of the tidal effect on the SW were also evident in the experiments with different tidal amplitudes. When the tidal amplitude was reduced in case A2-Q1, the USP contracted (Figure 2e; Table 3a). As a result of the reduced tidal effect, the SW intruded further inland; the distance to the SW toe increased by 17.5 cm compared with case A1-Q1. The opposite phenomena occurred when the tidal amplitude increased in case A3-Q1 (Figure 2f; Table 3a).

3.2. Laboratory-Scale Numerical Simulations

[23] The numerical model was calibrated at the laboratory scale by matching the simulated SFIs (including those of SW and USP) with the experimentally observed SFIs at the steady state for all tidal and nontidal cases. In the experiment, the boundary conditions were closely controlled and monitored. Therefore, the calibration only considered four input model parameters representing the properties of the porous medium: hydraulic conductivity (K), dispersivity (longitudinal, α_L and transverse, α_T), parameter a in the *van Genuchten* [1980] function and porosity (n). Although the hydraulic conductivity and porosity of the sand used were measured, both parameters were included in the calibration process due to measurement uncertainty. The numerical model was manually calibrated using trial-and-error methods to match the observed SFIs. The details of model calibration and sensitivity analysis are included in the auxiliary material.[1]

[24] The calibration results showed that the hydraulic conductivity and dispersivity had the most influence on the intrusion of the SW compared with the other calibration parameters (a and n; Figures A1a to A1h in auxiliary material). In contrast, the effect of hydraulic conductivity and dispersivity on the size of the USP was appeared to be less significant (Figures A1b, A1d, A1f and A1h). Typical values of the soil water retention parameters used in the van Genuchten function (inverse of air entry suction parameter a and exponent parameter m; Table 2) for sand were adopted in this study [*Carsel and Parrish*, 1988]. Only a was adjusted in calibration process as it affects largely the capillary rise. The results (Figure A1j) demonstrated that the capillary rise significantly influenced the extent of the USP—a smaller capillary rise leading to a larger USP. With the USP expanded, the extent of the SW intrusion was predicted to decrease (Figure A1j). However, the influence of capillary rise on the SW was not significant in the nontidal case (Figure A1i). The analysis showed that porosity had negligible influence on the SFIs (Figures A1k and A1l).

[1] Auxiliary materials are available in the HTML. doi:10.1029/2011WR010678.

Table 2. Parameters Values Adopted in Numerical Simulations

	Laboratory-Scale Model	Field-Scale Model (Following *Xin et al.* [2010])
	Domain	
Rectangular inland subdomain (m)	$\Delta x = 0.012$; $\Delta z = 0.0055$	$\Delta x = 1.5$; $\Delta z = 0.1/0.65$
Sloping intertidal subdomain (m)	$\Delta x = 0.0037$ $\Delta z = 0.00225 \sim 0.0055$ (varying from seaward to inland boundary)	$\Delta x = 0.33$ $\Delta z = 0.5 \sim 0.65$ (varying from seaward to inland boundary and further refinement of $\Delta z = 0.1$ near USP)
Rectangular seabed subdomain (m)	–	$\Delta x = 1.0$; $\Delta z = 0.1/0.5$
	Porous Medium Properties	
Hydraulic conductivity, K (m s^{-1})	5.0×10^{-3} [a]	1.157×10^{-4}
Porosity, n	0.46 (measured value)	0.45
Longitudinal dispersivity, α_L (m)	0.002[b]	0.5
Transverse dispersivity, α_T (m)	0.0004[b]	0.05
Diffusion Coefficient, D_f (m^2 s^{-1})	1.00×10^{-9} [b]	1.00×10^{-9}
Time step (s)	1	300
Exponent parameter, m[c]	2.68	2.68
Residual saturation, S_r [c]	0.1	0.1
Inverse of air entry suction parameter, a (m^{-1})[c]	5.9[b]	14.5[c]

[a]Adjusted from the measured value based on model calibration using data from case A1-Q1 and NT-Q1.
[b]Fitted values based on model calibration using data from case A1-Q1 and NT-Q1.
[c]Typical values [*Carsel and Parrish*, 1988] for soil water retention parameters used in the *van Genuchten* [1980] function, $S_w = S_r + (1 - S_r)\{1/[1 + (ap_c)^m]\}^{[(m-1)/m]}$ [*Voss and Provost*, 2002].

[25] In summary, values of the four model parameters calibrated were determined based on the steady and quasi-steady state results (Table 2). With these calibrated values, model simulations of the laboratory experiments provided a good match with the experimental observations. The salt-freshwater interfaces inferred from the simulated salt distributions agreed reasonably well with those based on the laboratory experiment images for both tidal and nontidal conditions (Figure 4). The numerical simulations also demonstrated that the tidal oscillations reduced the extent of saltwater intrusion in the aquifer.

[26] The numerical simulation of the physical experiment was also tested for the transient condition for case A1-Q1 using the calibrated parameter values (Table 2). The initial condition for the transient simulation corresponded with the laboratory experiment: freshwater in the aquifer with a constant water table set 5 cm higher than the MSL. The simulated transient behavior is similar to that observed in the physical model (Figure 3). Saltwater intruded into the aquifer across the vertical and sloping boundaries, forming the SW and USP which expanded with time until the (quasi) steady state (Figure 5). The simulated USP reached the quasi-steady state with an invariant half elliptic shape at ~30 min (Figure 5b); this was faster than the time shown by the physical model (~60 min; Figure 3d). A similar time lag was also evident near the UE of the SW (Figures 5b to 5d). In contrast, the numerical simulation matched well with the encroachment rate of the toe of SW (Figures 5b to 5e).

[27] The lag in the expansion of USP and encroachment of the SW's UE in the experiment may be attributed to the dilution of the saltwater in the nearshore zone. Although the reservoir was connected to a saltwater cycling system with a replenishment rate equal to the preset inland freshwater discharge, the initial 5 cm freshwater head above the MSL generated freshwater outflow across the beach surface at a greater rate than the designated inland freshwater flowrate (20 mL min^{-1}) at the beginning of experiment. This would

Table 3a. Results of Experiments and Numerical Simulations for Laboratory-Scale Models

Case	NT-Q1	NT-Q2	A1-Q1	A1-Q2	A2-Q1	A3-Q1
Toe of SW (cm)[a,b]	~52.0	~79.3	~18.9	~33.4	~36.4	~1.7
UE of SW (cm)[c]	~8.5	~5.7	~22.9	~23.0	~18.3	~30.1
Width of FDZ (cm)[d]	~8.9	~6.2	~11.1	~8.3	~11.6	~7.5
Area of USP (cm^2)	–	–	~182	~262	~64	~552
Q_T (ml min^{-1})[e]	–	–	15.6	18.3	6.5	25.9
RMSE (cm)[f]	4.25	2.15	3.53	9.09	4.24	3.95

[a]Measured landward from MS. Throughout, "~" indicates an approximate value.
[b]The toe of SW was obtained by extending the toe location linearly from the measuring tape to the bottom of the sand flume approximately 1 cm below the upper edge of tape (Figure 2).
[c]Measured seaward from MS.
[d]Measured along sloping beach surface.
[e]Results from numerical simulations.
[f]Root mean square error (RMSE) was calculated based on the difference between x coordinates of the interface given by the original or modified Glover solution and laboratory experiments or numerical simulations for a series of given z values.

Table 3b. Results of Numerical Simulation Results for Field-Scale Models

Case (FS-)	NT-Q1	NT-Q2	A1-Q1	A1-Q2
Toe of SW (m)[a]	39.0	84.9	10.5	19.7
UE of SW (m)[b]	4.9	2.6	16.7	19.9
Width of FDZ (m)[c]	4.9	2.6	7.2	4.9
Area of USP (m^2)	–	–	100.2	240.5
Q_T (m^3 d^{-1})[d]	–	–	0.206	0.271
RMSE (m)[e]	5.11	9.61	2.77	6.82

[a]Measured landward from MS.
[b]Measured seaward from MS.
[c]Measured along sloping beach surface.
[d]Results from numerical simulations.
[e]Root mean square error (RMSE) was calculated based on the difference between x coordinates of the interface given by the original or modified Glover solution and laboratory experiments or numerical simulations for a series of given z values.

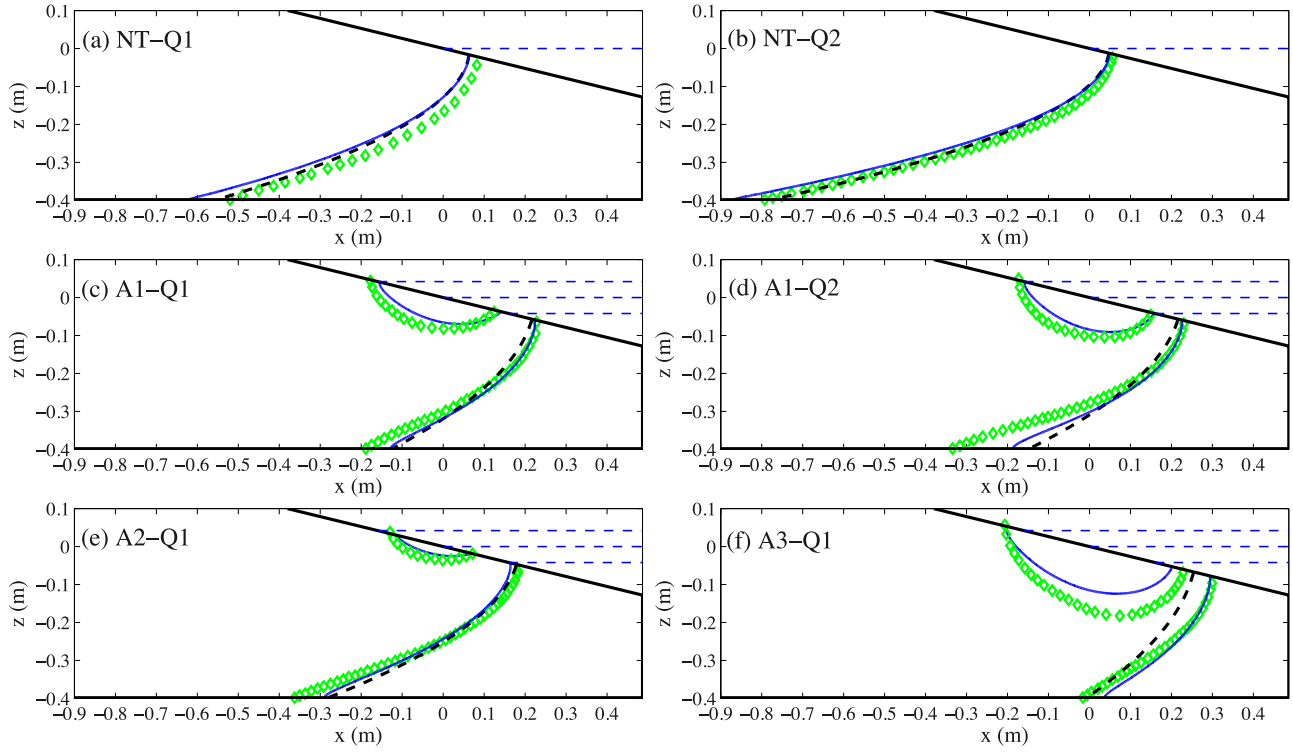

Figure 4. Comparison of the salt-freshwater interfaces (SFIs) based on numerical simulations, laboratory results and the Glover solutions for the study cases. Blue lines indicate 0.5 isochlors of the salt concentration from the numerical simulations; green diamonds denote the laboratory experiments; and black dashed lines indicate the prediction by the (a and b) Glover solution and (c, d, e, f) the modified Glover solution.

lead to a relatively intense dilution of the saltwater along the seaward boundary, weakening the density-driven flow and slowing down the saltwater intrusion. Because the diluted salt concentration was not measured, it was not possible to include the dilution effect in the numerical simulation. The numerical model assumed a constant salt concentration at 35 ppt in the reservoir and thus predicted faster developments of the SW and USP than observed in the experiment. As shown by the numerical simulation results, the freshwater outflow rate (initially >20 mL min^{-1}) at the seaward boundary decreased to ~20 mL min^{-1} after approximately 20 min. Without the interference of the initial saltwater dilution, the numerical and experimental results agreed well for the steady and quasi-steady state conditions (Figures 4).

3.3. Field-Scale Numerical Simulations

[28] The numerical investigations of the tidal influence on the SW were extended from the laboratory-scale to a field-scale shallow aquifer system to further explore the phenomena observed in the physical experiments. Four modeling cases (FS-NT-Q1, FS-NT-Q2, FS-A1-Q1, and FS-A1-Q2) were developed based on an unconfined aquifer system at Moreton Island, Australia (Figure 1c; Table 1). Two inland discharge rates were applied (Q1 = 0.21 m^3 d^{-1} and Q2 = 0.105 m^3 d^{-1}), for tidal (A1, tidal amplitude of 1 m) and nontidal (NT) conditions. The tidal influence on the SW was found to be similar to that observed in the laboratory-scale experiments and simulations. The SFI of the SW given by the 0.5 isochlor of the simulated salt distribution showed that for the nontidal condition, the toe of the SW intruded 39.0 m inland from the MS (at the steady state) for the high freshwater discharge case (Figure 6a; Table 3b). The UE of the SW was located 4.9 m seaward from the MS. With the tide, the toe of the SW retreated seaward and stopped at 10.5 m inland of the MS. The UE of the SW was also pushed seaward to 16.7 m from the MS, which was below the low tide mark (Figure 6c; Table 3b).

[29] For the simulations with reduced inland discharge, both the nontidal (FS-NT-Q2) and tidal cases (FS-A1-Q2) showed, as expected, greater extents of saltwater intrusion (Figures 6b and 6d), with the wedge toe advancing to 84.9 m and 19.7 m from the MS, respectively. Similar to the laboratory-scale simulations, for the tidal case, the increase in intrusion distance due to the reduction of freshwater discharge was significantly smaller: an increase of 9.2 m for the tidal case c.f. 45.9 m for the nontidal case (Table 3b). Again, this is due to the expansion of the USP under the reduced freshwater discharge.

3.4. Modified Glover Solution for Saltwater Wedge Incorporating Tidal Influence

[30] The laboratory and numerical experiments demonstrate the significant influence of the tide on seawater intrusion in unconfined coastal aquifers. With the tidal effect neglected, existing analytical solutions and numerical models over-predict the intrusion extent of the SW in unconfined aquifers subjected to tides. The Glover solution, for

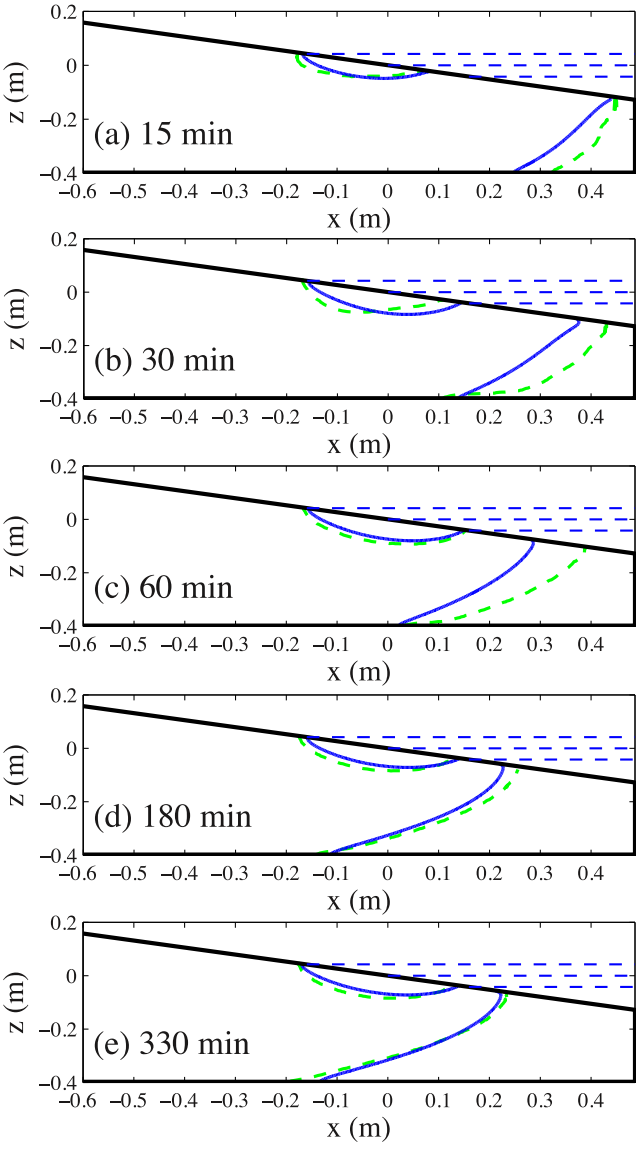

Figure 5. Transient simulation of case A1-Q1. Green dashed lines indicate the salt-freshwater interface from the laboratory experiments and blue continuous lines indicate the interface of 0.5 isochlors of the salt concentration from the numerical simulation results.

example, predicts well the SFI for the nontidal cases considered (Figures 4a, 4b, 6a, and 6b) but fails for the tidal cases.

[31] Tidal oscillations across the sloping beach surface generate hydraulic gradients that drive a pore water circulation system in the nearshore aquifer, with seawater infiltration in the upper part of the intertidal zone and exfiltration near the low tide mark. This tide-induced circulation recharges the unconfined aquifer in the intertidal zone and subsequently increases the total efflux from the aquifer to the sea over each tidal cycle. To modify the Glover solution to account for the tidal effect, we note that the additional seaward flow due to the tide restricts the density-driven seawater recirculation and hence extent of seawater intrusion. Based on this concept, we add the tide-induced discharge flow, Q_T (tide-induced circulation rate), to the Glover solution, i.e.,

$$x_{w,F+T} = \frac{Q_F + Q_T}{2\gamma K} \tag{4}$$

$$x_{I,F+T} = -(z^2 - 4x_{w,F+T}^2)\frac{\gamma K}{2(Q_F + Q_T)}. \tag{5}$$

The seaward retreat and steepening of the SFI observed in the tidal experiments can be predicted using equation (5). However, the outflow location predicted with equation (4) does not match the experimental results as tides cause this outflow zone to shift seaward to the low tide mark. To be consistent with this observation, the Glover solution was further modified as follows,

$$x_{I,F+T} = -[z^2 - 4x_{w,F+T}(x_{w,F} + D_{LTM})]\frac{\gamma K}{2(Q_F + Q_T)}, \tag{6}$$

where D_{LTM} [L] is the horizontal distance of low tide mark from the MS. To test equation (6) against the experimental and numerical results, we determined Q_T based on the simulated tidal circulations rate (net influx across the upper part of the beach over the tidal cycle): 15.6 mL min^{-1} for case A1-Q1, 6.5 mL min^{-1} for case A2-Q1, 25.9 mL min^{-1} for case A3-Q1 and 18.3 mL min^{-1} for case A1-Q2 (Table 3a). D_{LTM} [L] was determined based on the tidal amplitude and beach slope (note that the Glover solution does not consider the beach slope). The predictions by the modified Glover solution, (equation (6)), agreed reasonably well with the experimental and numerical results of the laboratory-scale model (Figures 4c to 4f). To further assess the agreement, a root mean square error (RMSE) was calculated for each case, based on the difference between x coordinates of the interface given by the (original or modified) Glover solution and laboratory experiments or numerical simulations for a series of given z values (Table 3). The RMSE for the prediction by the original Glover solution in nontidal cases NT-Q1 and NT-Q2 were calculated to be 4.25 cm and 2.15 cm, respectively, while the RMSE for the prediction by the modified Glover solution for tidal cases A1-Q1, A1-Q2, A2-Q1 and A3-Q1 were 3.53 cm, 9.09 cm, 4.24 cm and 3.95 cm, respectively. The modified Glover solution also provided good prediction of the location of the SW for the field-scale model (Figures 6c and 6d). The RMSE for the prediction by the Glover solution in nontidal cases FS-NT-Q1 and FS-NT-Q2 were 5.11 m and 9.61 m, respectively, while the RMSE from applying the modified Glover solution for tidal cases FS-A1-Q1 and FS-A1-Q2 were 2.77 m and 6.82 m, respectively. If the tidal influence was neglected in the Glover solution, the RMSE for the predicted interface for FS-A1-Q1 and FS-A1-Q2 increased by an order of magnitude to 25.0 m and 55.8 m, respectively.

4. Conclusion

[32] Tidal influence on the salt distribution in unconfined coastal aquifers was previously thought to be limited to the near-shore area with the formation of the USP. This work shows that the tide also influences the extent of seawater intrusion further inland. Laboratory experiments and numerical simulations demonstrate that tidal effects can cause

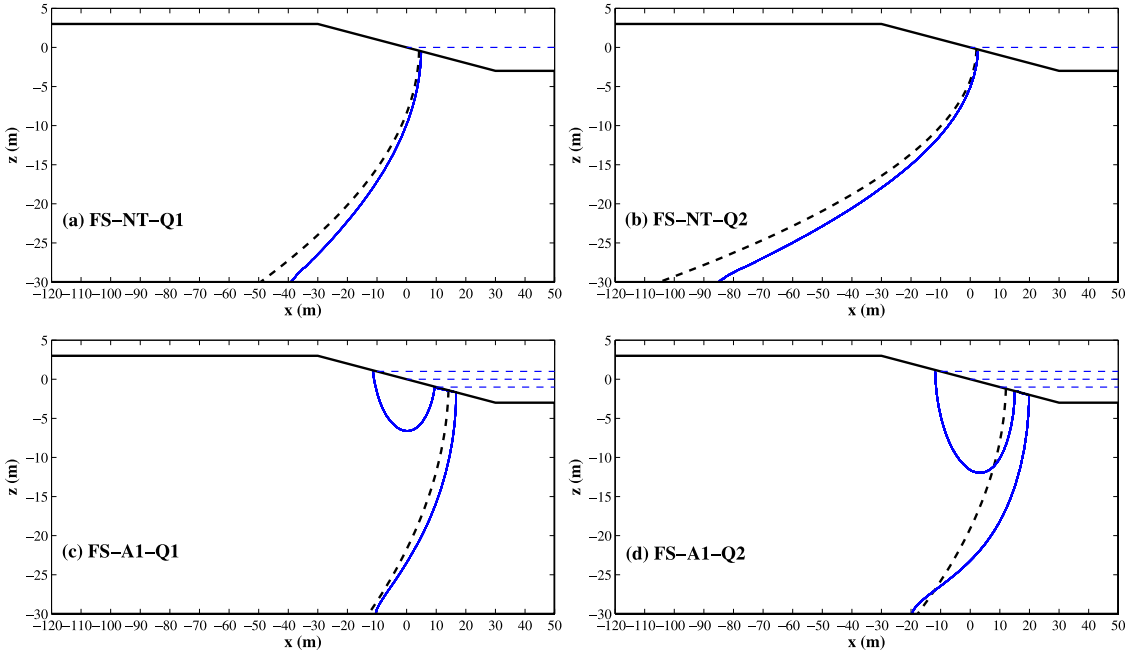

Figure 6. Comparison of salt-freshwater interfaces (SFIs) based on numerical simulations and the Glover solutions for the field-scale study cases. Blue lines indicate the 0.5 contours of the salt concentration from the numerical simulations. Black dashed lines indicate the prediction of the Glover solution (a and b) and the modified Glover solution (c and d).

a significant reduction of seawater intrusion in an unconfined coastal aquifer. Tide-induced circulation across the seaward boundary increases the total discharge from the aquifer to the sea, which in turn restricts the density-driven circulation and the resulting SW in the aquifer.

[33] The tidal effects on the SW are two: a seaward shift of the FDZ to the low tide mark and steepening of the wedge interface. The Glover solution was modified to incorporate these effects. While the modified Glover solution was found to predict well the experimental and numerical simulation results, the prediction relied on the numerical simulation results to determine the tidal circulation rate Q_T as part of the modified solution. Attempts have been made to quantify this circulation rate as part of submarine groundwater discharge from field investigations [*Taniguchi*, 2002; *Taniguchi et al.*, 2002; *Burnett et al.*, 2006] and numerical modeling [*Robinson et al.*, 2007a] but no simple quantification is available, unlike Q_F and K which can be estimated based on aquifer recharge and pumping test data, respectively. Previous numerical simulations reveal complex behavior of the tidal circulation depending on the tidal amplitude, inland freshwater discharge rate and aquifer properties [*Robinson et al.*, 2007b]. Further understanding of the inter-relationship among these factors is required for estimating Q_T and resulting effects on the SW.

[34] A number of assumptions have been made in this study, including along-shore uniformity (2-D physical and numerical models) and aquifer homogeneity. In reality, three-dimensionality and heterogeneity of the aquifer would lead to more complex flow and salt transport, and hence SW behavior. A further complication can be due to mixed landward boundary conditions controlled by fixed flux at some locations and fixed head at others. Fixed head landward boundary combined with tidal water table overheight may produce less freshwater discharge to the shore which would intensify the saltwater intrusion even with the tidal moderation (detailed discussion is included in the auxiliary material). Further studies are needed to examine these complex, combined effects on saltwater intrusion in unconfined coastal aquifers. As a starting point, the present study has illustrated the significance of the tide in modulating the salt distribution in unconfined coastal aquifers not only within but also landward of the intertidal zone.

[35] **Acknowledgments.** This research was supported by an Australian Research Council Discovery grant (DP0988718). The laboratory facilities are provided by Centre for Eco-Environmental Modeling at Hohai University. W.K. Kuan acknowledges the financial assistance of Malaysia Higher Education Scholarship. The authors acknowledge Li Xu and Chengji Shen of Hohai University for their assistance with the laboratory experiments.

References

Abarca, E., and T. P. Clement (2009), A novel approach for characterizing the mixing zone of a saltwater wedge, *Geophys. Res. Lett.*, *36*, L06402, doi:10.1029/2008GL036995.

Ataie-Ashtiani, B., R. E. Volker, and D. A. Lockington (1999), Tidal effects on sea water intrusion in unconfined aquifers, *J. Hydrol.*, *216*, 17–31, doi:10.1016/s0022-1694(98)00275-3.

Barlow, P. M., and E. G. Reichard (2010), Saltwater intrusion in coastal regions of North America, *Hydrogeol. J.*, *18*, 247–260, doi:10.1007/s10040-009-0514-3.

Bear, J., and H. D. C. Alexander (2010), *Modeling Groundwater Flow and Contaminant Transport, Theory Appl. Transp. Porous Media*, vol. 23, Springer, Dordrecht, Netherlands.

Bear, J., A. H.-D. Cheng, S. Sorek, D. Ouazar, and I. Herrera (Eds.) (1999), *Seawater Intrusion in Coastal Aquifers: Concepts, Methods, and Practices*, Kluwer, Dordrecht, Netherlands.

Bobba, A. G. (1993), Mathematical models for saltwater intrusion in coastal aquifers, *Water Resour. Manage.*, *7*, 3–37.

Boufadel, M. C. (2000), A mechanistic study of nonlinear solute transport in a groundwater-surface water system under steady state and transient hydraulic conditions, *Water Resour. Res.*, *36*, 2549–2565.

Burnett, W. C., et al. (2006), Quantifying submarine groundwater discharge in the coastal zone via multiple methods, *Sci. Total Environ.*, *367*, 498–543, doi:10.1016/j.scitotenv.2006.05.009.

Carsel, R. F., and R. S. Parrish (1988), Developing joint probability distributions of soil water retention characteristics, *Water Resour. Res.*, *24*, 755–769.

Cartwright, N., P. Nielsen, and S. Dunn (2003), Water table waves in an unconfined aquifer: Experiments and modeling, *Water Resour. Res.*, *39*(12), 1330, doi:10.1029/2003WR002185.

Cartwright, N., P. Nielsen, and L. Li (2004), Experimental observations of watertable waves in an unconfined aquifer with a sloping boundary, *Adv. Water Resour.*, *27*, 991–1004, doi:10.1016/j.advwatres.2004.08.006.

Chang, S. W., T. P. Clement, M. J. Simpson, and K.-K. Lee (2011), Does sea-level rise have an impact on saltwater intrusion?, *Adv. Water Resour.*, *34*, 1283–1291, doi:10.1016/j.advwatres.2011.06.006.

Chen, B. F., and S. M. Hsu (2004), Numerical study of tidal effects on seawater intrusion in confined and unconfined aquifers by time-independent finite-difference method, *J. Waterw. Port Coastal Ocean Eng.*, *130*, 191–206.

Collins, R. E. (1961), *Flow of Fluids Through Porous Materials*, Reinhold Pub. Corp., New York.

Dale, R. K., and D. C. Miller (2007), Spatial and temporal patterns of salinity and temperature at an intertidal groundwater seep, *Estuarine Coastal Shelf Sci.*, *72*, 283–298, doi:10.1016/j.ecss.2006.10.024.

Glover, R. E. (1959), The pattern of fresh-water flow in a coastal aquifer, *J. Geophys. Res.*, *64*, 457–459.

Goswami, R. R., and T. P. Clement (2007), Laboratory-scale investigation of saltwater intrusion dynamics, *Water Resour. Res.*, *43*, W04418, doi:10.1029/2006WR005151.

Inouchi, K., Y. Kishi, and T. Kakinuma (1990), The motion of coastal groundwater response to the tide, *J. Hydrol.*, *115*, 165–191.

Lanyon, J., I. Eliot, and D. Clarke (1982), Groundwater-level variation during semidiurnal spring tidal cycles on a sandy beach, *Aust. J. Mar. Freshwater Res.*, *33*, 377–400.

Li, L., D. A. Barry, and C. B. Pattiaratchi (1997), Numerical modelling of tide-induced beach water table fluctuations, *Coastal Eng.*, *30*, 105–123.

Luyun, R., K. Momii, and K. Nakagawa (2009), Laboratory-scale saltwater behavior due to subsurface cutoff wall, *J. Hydrol.*, *377*, 227–236, doi:10.1016/j.jhydrol.2009.08.019.

Mao, X., P. Enot, D. A. Barry, L. Li, A. Binley, and D. S. Jeng (2006), Tidal influence on behaviour of a coastal aquifer adjacent to a low-relief estuary, *J. Hydrol.*, *327*, 110–127, doi:10.1016/j.jhydrol.2005.11.030.

Meier, M. F., M. B. Dyurgerov, U. K. Rick, S. O'Neel, W. T. Pfeffer, R. S. Anderson, S. P. Anderson, and A. F. Glazovsky (2007), Glaciers dominate eustatic sea-level rise in the 21st century, *Science*, *317*, 1064–1067, doi:10.1126/science.1143906.

Nielsen, P. (1990), Tidal dynamics of the water table in beaches, *Water Resour. Res.*, *26*, 2127–2134.

Pfeffer, W., J. Harper, and S. O'neel (2008), Kinematic constraints on glacier contributions to 21st-century sea-level rise, *Science*, *321*, 1340.

Reilly, T. E., and A. S. Goodman (1985), Quantitative analysis of saltwater fresh-water relationships in groundwater systems—A historical perspective, *J. Hydrol.*, *80*, 125–160.

Robinson, C., B. Gibbes, and L. Li (2006), Driving mechanisms for groundwater flow and salt transport in a subterranean estuary, *Geophys. Res. Lett.*, *33*, L03402, doi:10.1029/2005GL025247.

Robinson, C., L. Li, and D. A. Barry (2007a), Effect of tidal forcing on a subterranean estuary, *Adv. Water Resour.*, *30*, 851–865, doi:10.1016/j.advwatres.2006.07.006.

Robinson, C., L. Li, and H. Prommer (2007b), Tide-induced recirculation across the aquifer-ocean interface, *Water Resour. Res.*, *43*, W07428, doi:10.1029/2006WR005679.

Robinson, C., B. Gibbes, H. Carey, and L. Li (2007c), Salt-freshwater dynamics in a subterranean estuary over a spring-neap tidal cycle, *J. Geophys. Res.*, *112*, C09007, doi:10.1029/2006JC003888.

Robinson, M., D. Gallagher, and W. Reay (1998), Field observations of tidal and seasonal variations in ground water discharge to tidal estuarine surface water, *Ground Water Monit. Rem.*, *18*, 83–92.

Taniguchi, M. (2002), Tidal effects on submarine groundwater discharge into the ocean, *Geophys. Res. Lett.*, *29*(12), 1561, doi:10.1029/2002GL014987.

Taniguchi, M., W. C. Burnett, J. E. Cable, and J. V. Turner (2002), Investigation of submarine groundwater discharge, *Hydrol. Processes*, *16*, 2115–2129, doi:10.1002/hyp.1145.

Turner, I. L., B. P. Coates, and R. I. Acworth (1997), Tides, waves and the super-elevation of groundwater at the coast, *J. Coastal Res.*, *13*, 46–60.

Vandenbohede, A., and L. Lebbe (2006), Occurrence of salt water above fresh water in dynamic equilibrium in a coastal groundwater flow system near De Panne, Belgium, *Hydrogeol. J.*, *14*, 462–472.

Vandenbohede, A., and L. Lebbe (2007), Effects of tides on a sloping shore: Groundwater dynamics and propagation of the tidal wave, *Hydrogeol. J.*, *15*, 645–658, doi:10.1007/s10040-006-0128-y.

van Genuchten, M. T. (1980), A closed-form equation for predicting the hydraulic conductivity of unsaturated soils, *Soil Sci. Soc. Am. J.*, *44*, 892–898.

Voss, C. I., and A. M. Provost (2002), SUTRA, a model for saturated-unsaturated variable density ground-water flow with energy or solute transport, *U.S. Geol. Surv. Open File Rep. 02-4231*, 250 pp.

Werner, A. D., and D. A. Lockington (2006), Tidal impacts on riparian salinities near estuaries, *J. Hydrol.*, *328*, 511–522, doi:10.1016/j.jhydrol.2005.12.011.

Werner, A. D., and C. T. Simmons (2009), Impact of sea-level rise on sea water intrusion in coastal aquifers, *Ground Water*, *47*, 197–204, doi:10.1111/j.1745-6584.2008.00535.x.

Xin, P., C. Robinson, L. Li, D. A. Barry, and R. Bakhtyar (2010), Effects of wave forcing on a subterranean estuary, *Water Resour. Res.*, *46*, W12505, doi:10.1029/2010WR009632.

Zhang, Q., R. E. Volker, and D. A. Lockington (2002), Experimental investigation of contaminant transport in coastal groundwater, *Adv. Environ. Res.*, *6*, 229–237.

B. Gibbes, School of Civil Engineering, University of Queensland, St. Lucia, Qld 4072, Australia. (b.gibbes@uq.edu.au)

G. Jin, State Key Laboratory of Hydrology, Water Resources and Hydraulic Engineering, Hohai University, 1 Xikang Rd., Nanjing, China. (jingq@hhu.edu.cn)

W. K. Kuan, L. Li, and P. Xin, National Centre for Groundwater Research and Training, School of Civil Engineering, University of Queensland, St. Lucia, Qld 4072, Australia. (wkkuan@uq.edu.au; l.li@uq.edu.au; p.xin@uq.edu.au)

C. Robinson, Department of Civil and Environmental Engineering, University of Western Ontario, London, ON N6A5B9, Canada. (crobinson@eng.uwo.ca)